Astronomy 320
Final Observing Report
Nicholas O'Karma

Preface

In order to avoid redundancy, let it be known that my lab partner is Lazar Buntic; use of "we" refers to Mr. Buntic and myself. It should also be understood that we used the 24-inch PlaneWave telescope for each observing exercise.

Contents

Exercise A: CCD Characteristics: Read Noise and Dark Current

Experimental Procedure

We prepared to take dark and bias frames by ensuring that the interior of the dome was as dark as possible. With cooling disabled, we exposed the camera for 0.1, 0.3, 1, 3, 10 and 30 seconds. We then set the cooler temperature to reach -30°C. While it fell, we took a 20 s dark exposure followed by a 1 s light exposure every 60 seconds, repeating 50 times. Finally, with the cooler still at -30°C, we took 30 bias frames (i.e. dark frames with 0.12 s exposure time).

Analysis and Results

I first determined the readout noise of the CCD by finding the standard deviations of pixel values in a small, uniform region (a square with 100 pixel long sides) of each bias frame. This method leads to an average read noise of 15.729 ± 0.119 DN. The difference between the standard deviations of the bias images and the read noise measurements is quite consistent, with a mean difference of 8.070 ± 0.184 DN.

I determined the read noise again by subtracting the average bias from each bias frame, then finding their standard deviations. In doing this, I found the average read noise to be 15.379 ± 0.258 DN. This result is slightly less precise than the previous. Figure A.1 summarizes these findings.

Read Noise from bias region	Stdev of bias frame	Read Noise from bias subtraction
15.680	23.72	15.300
15.670	23.74	15.230
15.650	23.73	15.260
15.670	23.76	15.260
15.640	23.75	15.290
15.730	23.82	15.430
15.930	23.73	15.310
15.910	23.73	15.280
15.800	23.74	15.250
15.620	23.73	15.270
15.760	23.72	15.250
15.840	24.07	15.820
15.650	23.73	15.290
15.660	23.71	15.240
15.690	23.73	15.240
15.610	24.25	16.040
15.750	23.72	15.280
15.550	23.76	15.340
15.890	23.73	15.290

15.650	23.73	15.260
15.840	23.73	15.260
15.480	23.73	15.290
15.540	23.72	15.310
15.740	23.73	15.320
15.910	24.03	15.730
15.770	23.75	15.250
15.800	23.75	15.300
15.880	23.74	15.310
15.700	23.77	15.340
15.860	24.41	16.330
Average: 15.729		15.379
Standard Deviation : 0.119		0.258

Figure A.1 : Table summarizing the readout noise calculation.

Running *imexam* → [*l*] on one of our bias images, I produced a plot of pixel values in a selected row vs. the columns across the detector (Fig. A.2). This plot shows that the image fluctuations across the CCD are quite minimal and well-contained. At the starting (left) side of the bias images, there is a column of totally black pixels, separated from a larger column of totally white pixels; this behavior is likely due to the way the image is read out in such a short span of time, and it is exhibited on this plot.

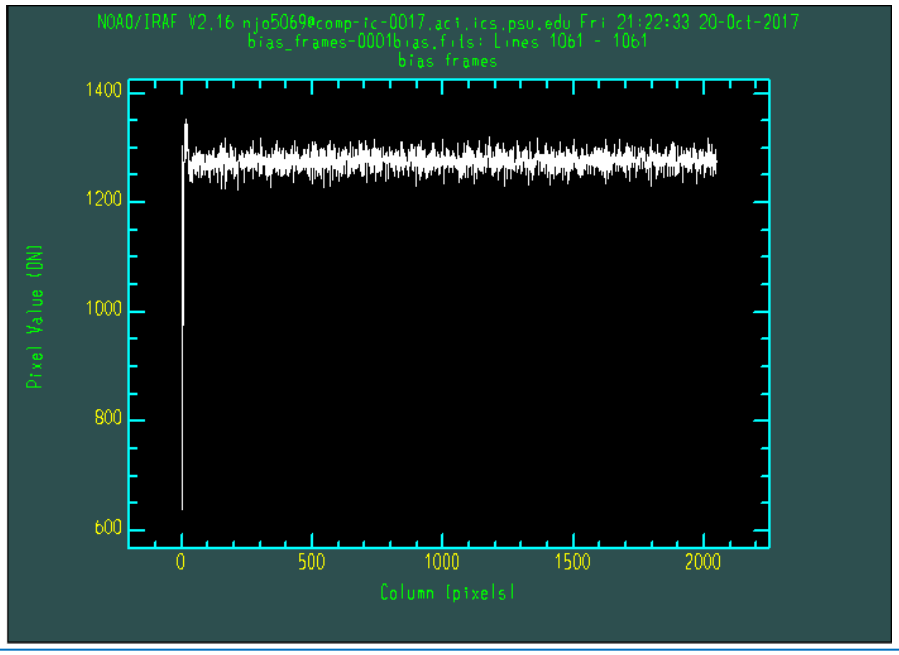

Figure A.2 : Pixel values in DN vs. the column number for an arbitrary row for a bias frame.

Using *imstat*, I found the mean DN value for each of the exposures. Knowing the gain of the camera (see Exercise B) allowed me to find the dark charge in the images by simply multiplying the gain (e^-/DN) and the mean DN; the dark current follows as the charge over the exposure time. Figure A.3 summarizes the results.

Mean DN	Dark Charge (e^-/pixel)	Dark Current (e^-/pixel*s)
3826.0	2590.5	129.53
3134.0	2122.0	106.10
2595.0	1757.0	87.852
2190.0	1482.8	74.141
1899.0	1285.8	64.289
1696.0	1148.3	57.417
1557.0	1054.2	52.711
1463.0	990.58	49.529
1399.0	947.24	47.362
1356.0	918.13	45.906
1327.0	898.49	44.925
1307.0	884.95	44.248
1293.0	875.47	43.774
1284.0	869.38	43.469
1277.0	864.64	43.232
1272.0	861.25	43.063
1269.0	859.22	42.961
1267.0	857.87	42.893
1265.0	856.51	42.826
1264.0	855.84	42.792
1263.0	855.16	42.758
1262	854.48	42.724
1261	853.81	42.690
1260	853.13	42.656
		Mean = 54.993
Gain = 0.677 e-/DN	**Exposure Time = 20 s**	± 22.67

Figure A.3 : This table lists the dark charge and current measurements along with the numbers used to obtain them.

I found that dark charge varies linearly with exposure time (Fig. A.4). This result was expected, since exposing the CCD for a longer time allows more thermal electrons to trigger a count.

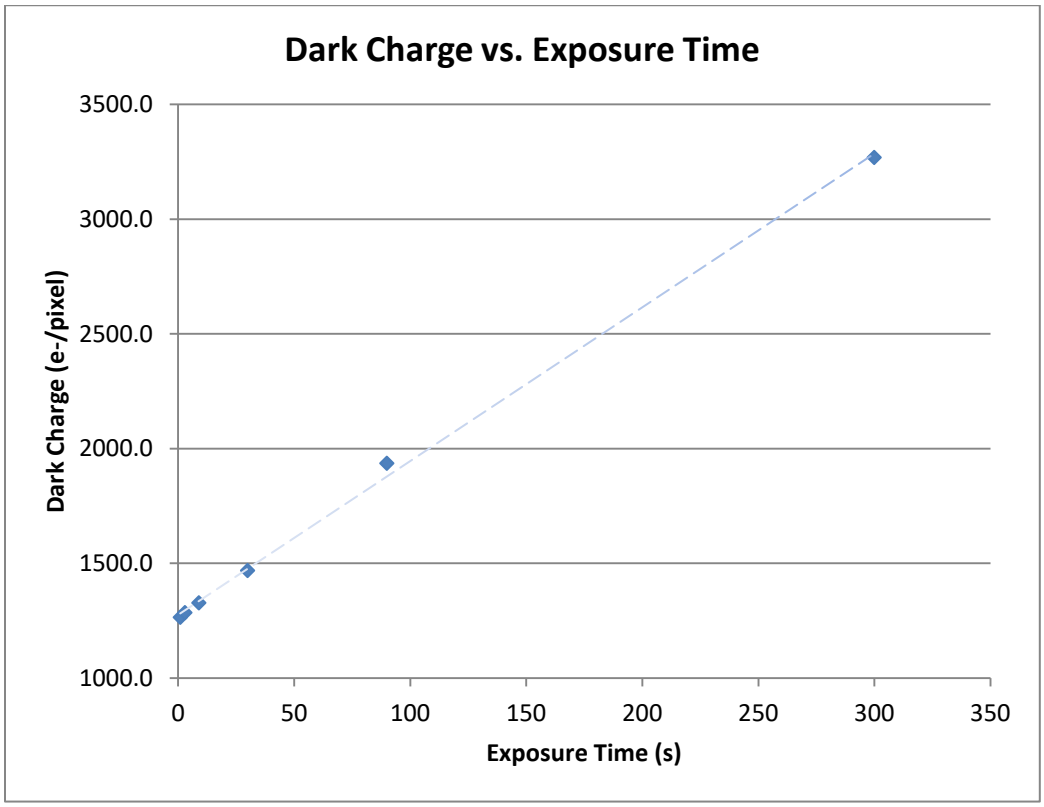

Figure A.4 : Dark charge in bias frames as a function of exposure time.

Using the dark exposures at decreasing temperature, I plotted the dark charge as a function of temperature (Fig. A.5).

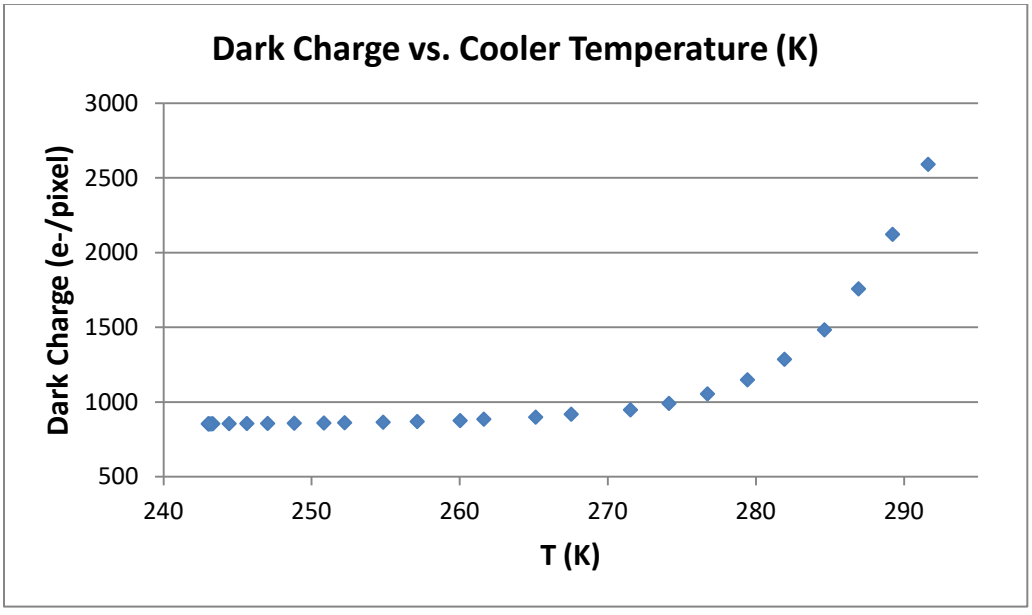

Figure A.5 : Dark Charge as a function of the cooler temperature in Kelvin.

Knowing that $I(T) \propto e^{-1/T}$, I can conclude that the temperature dependence *is* consistent with dark current from thermal electrons by looking at this graph. Plotting the natural log of the dark charge as a function of inverse temperature scaled by 1000 (Fig. A.6) results in a straight line with negative slope, as one would expect.

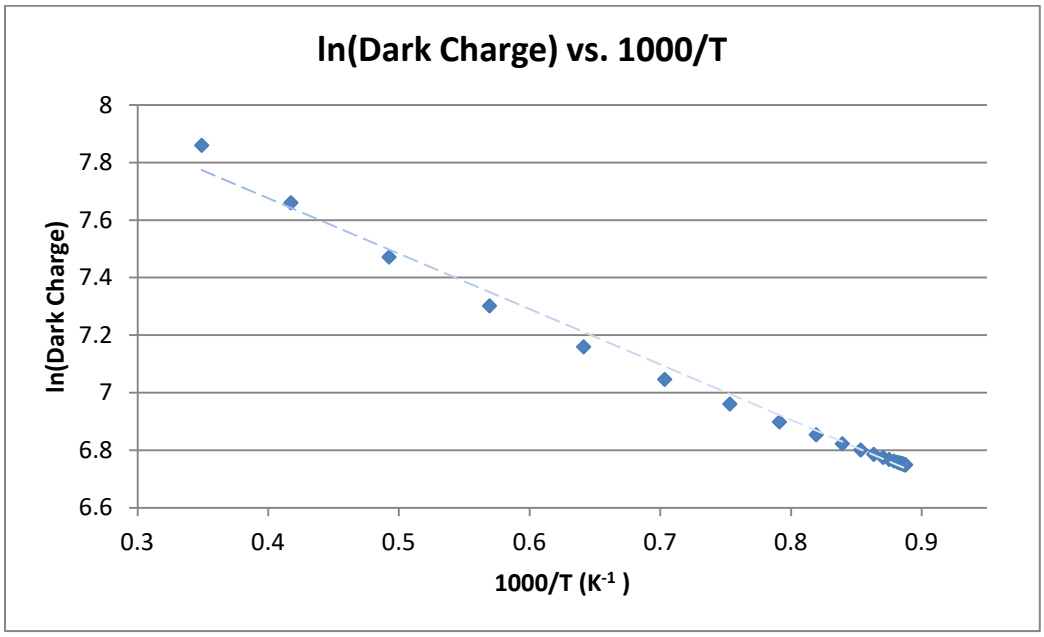

Figure A.6: The natural log of the dark charge as a function of 1000 times the inverse of the cooler temperature in Kelvin.

Exercise B: Flat Fields: Dome and Sky Flats and the CCD Gain

Experimental Procedure

We prepared to take sky flats by exposing the camera for 6 s every minute until the maximum DN given by the histograms produced in MaximDL was well below saturation. We then obtained the flats by taking thirty consecutive 6 s exposures of flat patches of sky and cloud (Fig B.2). Next, we repositioned the telescope and dome in order to begin taking dome flats. We tuned the LED current to 1.24 mA and voltage to 10.5 V, then took twenty 0.2 and 10 s dome flats (Fig. B.3). Finally, we collected data for the photon transfer curve, taking many exposures at increasing lengths, ensuring that our DN ranged spanned at least a factor of ten. Despite exposing the camera for 165 s, we were unable to obtain a saturated dome flat.

Analysis and Results

I generated a photon transfer curve (Fig. B.1) for the CCD by plotting the standard deviation as a function of the mean DN of our dome flats at increasing exposure length. There is no full well cutoff because we did not saturate any of our dome flats.

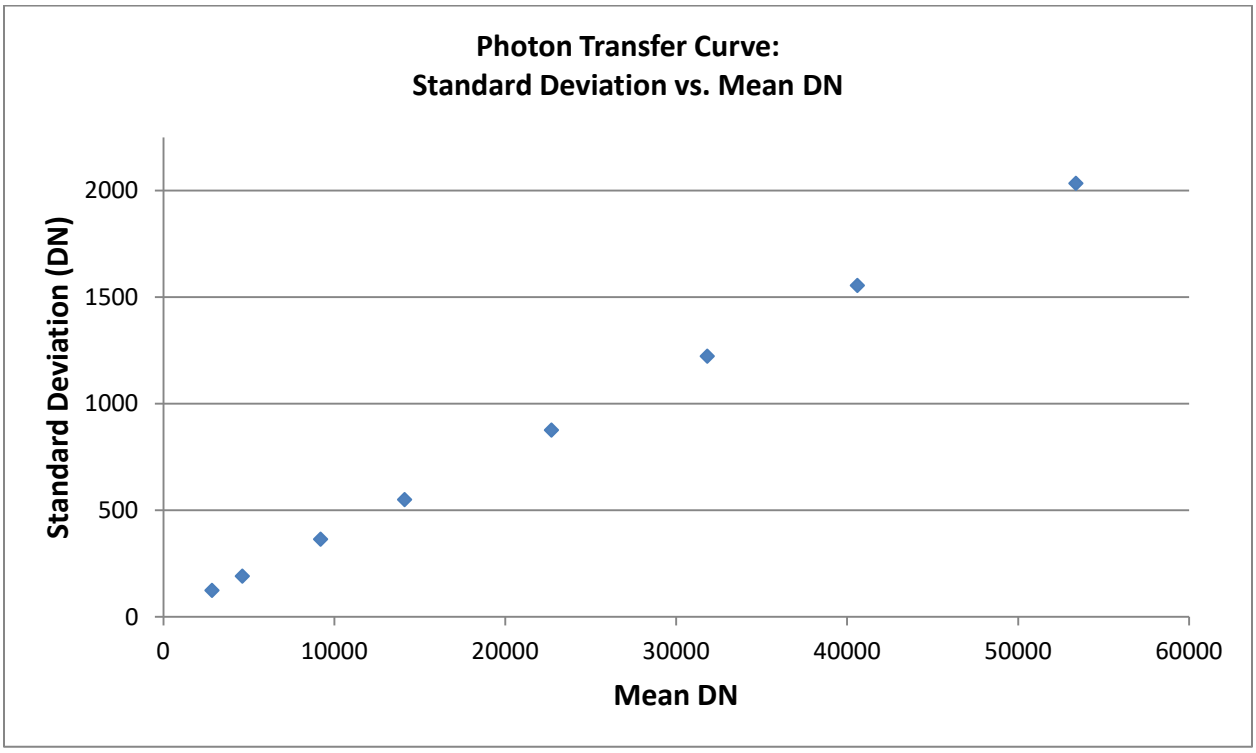

Figure B.1 : A photon transfer curve for the 24-inch telescope. Note there is no full well cutoff present due to the lack of a saturated dome flat in our data. The standard deviation from the mean slope is used as the error.

Figure B.2 : A 6 s sky flat exposure.

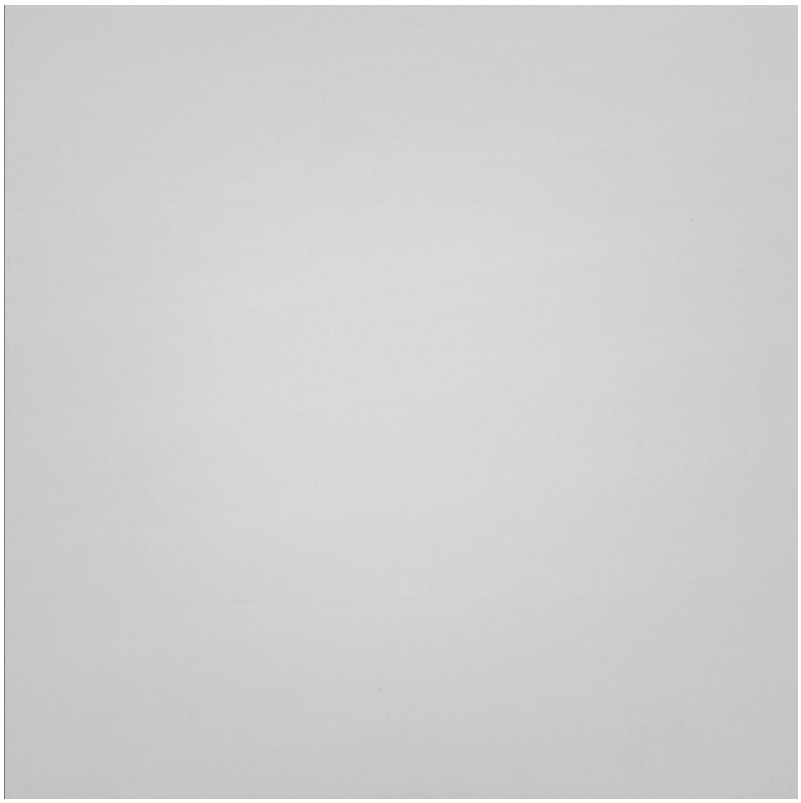

Figure B.3 : A 10 s dome flat exposure.

Solving the CCD Noise Equation for the gain yields the equation

$$Gain = \frac{S_{Sky}}{\sigma^2_{Sky} - \sigma^2_{ReadNoise}} \qquad \text{(Eq. 1)}$$

where S denotes the mean signal and sigma denotes the standard deviation. To actually calculate the gain, I chose a uniform square patch on our sky flats centered at coordinates (1200, 1200) with a side length of 100 pixels, then ran *imstat* over this region for each exposure to find its mean DN and corresponding standard deviation. I calculated the gain using Eq. 1 for each exposure, and found the average gain to be 0.677 ± 0.046 e^-/DN. The standard deviation from the mean gain is used as the uncertainty.

S_{sky} (DN)	σ_{sky} (DN)	σ_{RN} (DN)	Gain (e^-/DN)
33341	227.4	0.258	0.645
34966	238.2		0.616
35066	236.5		0.627
33650	235.1		0.609
32481	226.6		0.633
33511	228.9		0.640
33793	230.1		0.638
34050	232.6		0.629
32840	231.9		0.611
30671	217.7		0.647
29767	214.3		0.648
26167	208.0		0.605
25111	190.0		0.696
25405	191.9		0.690
24148	188.5		0.680
23772	182.2		0.716
25298	189.9		0.702
27217	202.5		0.664
26476	196.4		0.686
24271	187.3		0.692
20159	174.3		0.664
18958	159.2		0.748
17749	157.2		0.718
17442	150.8		0.767
18512	157.2		0.749
20846	168.8		0.732
21124	172.2		0.712
21554	172.7		0.723
21496	173.0		0.718

21267	173.1		0.710
		Average Gain:	0.677
		Error ±	0.046

Figure B.4 : This table summarizes the pertinent values used for the gain calculation

Using *imexam* → [*l*], I generated 1-D plots of the columnal illumination of the field of view for 200ms sky and dome flats (Figures B.5, B.6)

Figure B.5 : Intensity of an arbitrarily selected row vs. the column number across the detector for a 200ms sky flat.

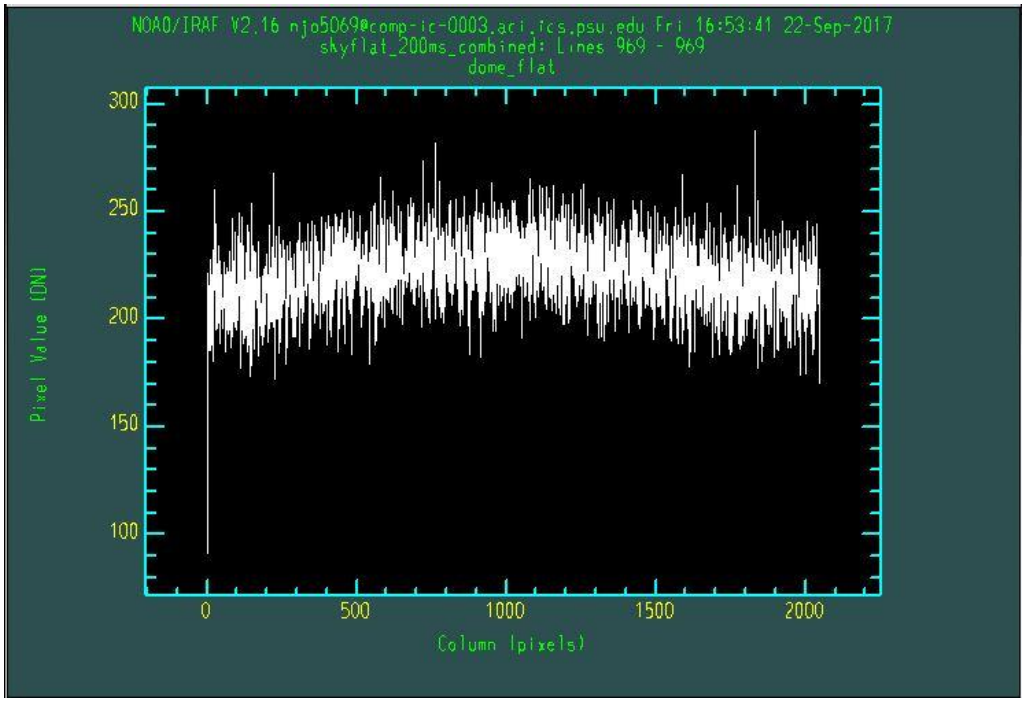

Figure B.6 : Intensity of an arbitrarily selected row vs. the column number across the detector for a 200ms dome flat.

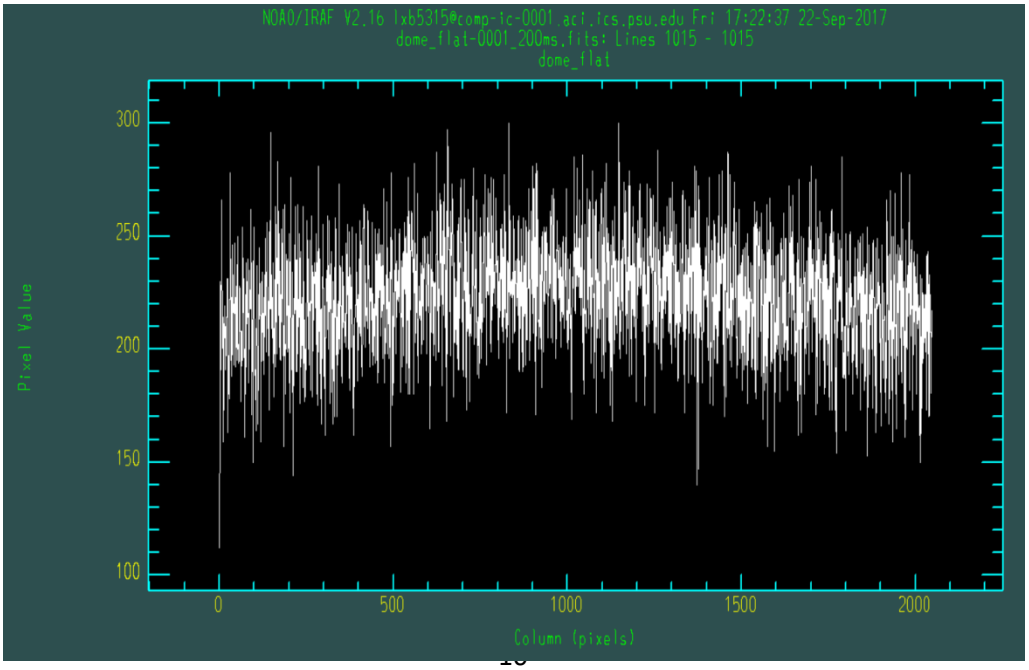

In regards to comparing sky and dome flats: One can take dome flats at any time, while sky flats need to be taken at the right time to avoid either saturating the image (when the physical setting is too bright) or exposing an actual image of stars (too dark). What's more, one has more control over the illumination level when taking dome flats because of the adjustable LEDs, but this also means that the light is distributed less naturally (uniformly) when compared to sky flats.

The gain of the CCD measures the conversion from electrons to DN, and it determines which component involved in producing the image saturates first. The ADC is usually the first component to saturate, as it can only handle 65,535 (2^{16} - 1) DN. Next to saturate is the CCD full well, which can hold up to 100,000 DN. The analog electronics can saturate if the gain and incoming signal are both high, but I see no reason to produce a CCD with such high gain; perhaps we could saturate the electronics if we pointed the telescope at the sun.

Exercise C: Photometry of Stars: Image Quality and Photometric Uncertainty

Experimental Procedure

Upon preparing the telescope to take data, we focused the camera by taking short exposures, then slewed to 54 Aquilae. We familiarized ourselves with PWI3 and set the focus position to 18,000 μm, took an exposure and noted the ring-like appearance of the out of focus star. With the R filter in place, we took 0.1 s exposures of the star at focus positions ranging from 16,000 to 21,250 μm. We refocused on a fainter star in the field, then took exposures of it until it saturated. We found that as a star saturates, it progressively becomes more circular until the circle fills and additional counts form up in a stereotypical star pattern. Without moving the telescope or focuser, we concluded our observations by taking ten consecutive 3.25 second exposures to use for our photometric measurements. We later realized that we had not turned on automatic dark subtraction for the majority of our star images.

Analysis and Results

I obtained values for the FWHM of a target star in each exposure at varying focal length in order to plot them against the focal length (Fig. C.1). For the focused exposures of this star, I found these values using *imexam* → [*Period*] (radial profile). For the unfocused images, I followed the procedure of determining the maximum DN value and finding two points on opposite sides of the star with half of this value, then taking the distance between the points to be the FWHM.

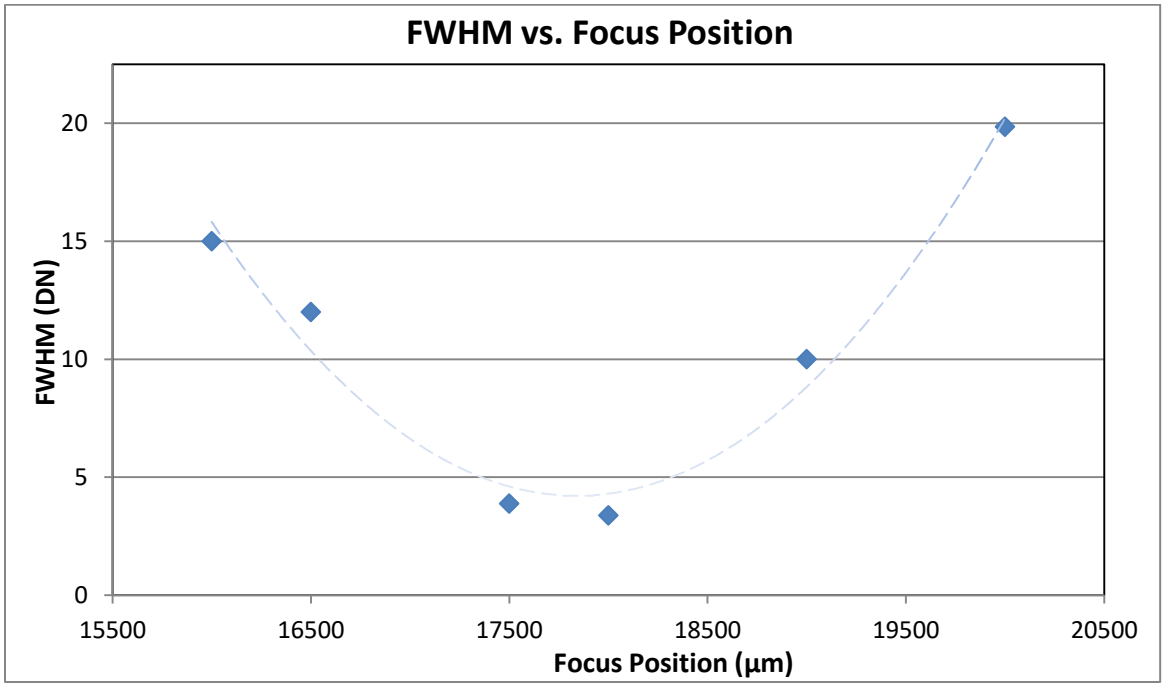

Figure C.1: Full Width at Half Maximum as a function of the position of the focus mechanism

This plot clearly shows how when the telescope is unfocused, the image of the star is stretched across the detector, resulting in a larger FWHM. The images taken at 17,500 and 18,000 μm were visibly the most in-focus, and this is shown in this plot.

Using *imexam* I found the FWHM of our target star in each exposure and plotted it against the exposure time (Fig. C.2). The plot exhibits a positive trend, which I expected because of how the CCD deals with increasing saturation by expanding the size of the star. The mean FWHM was 3.66 DN and the standard deviation from this mean is used as the error.

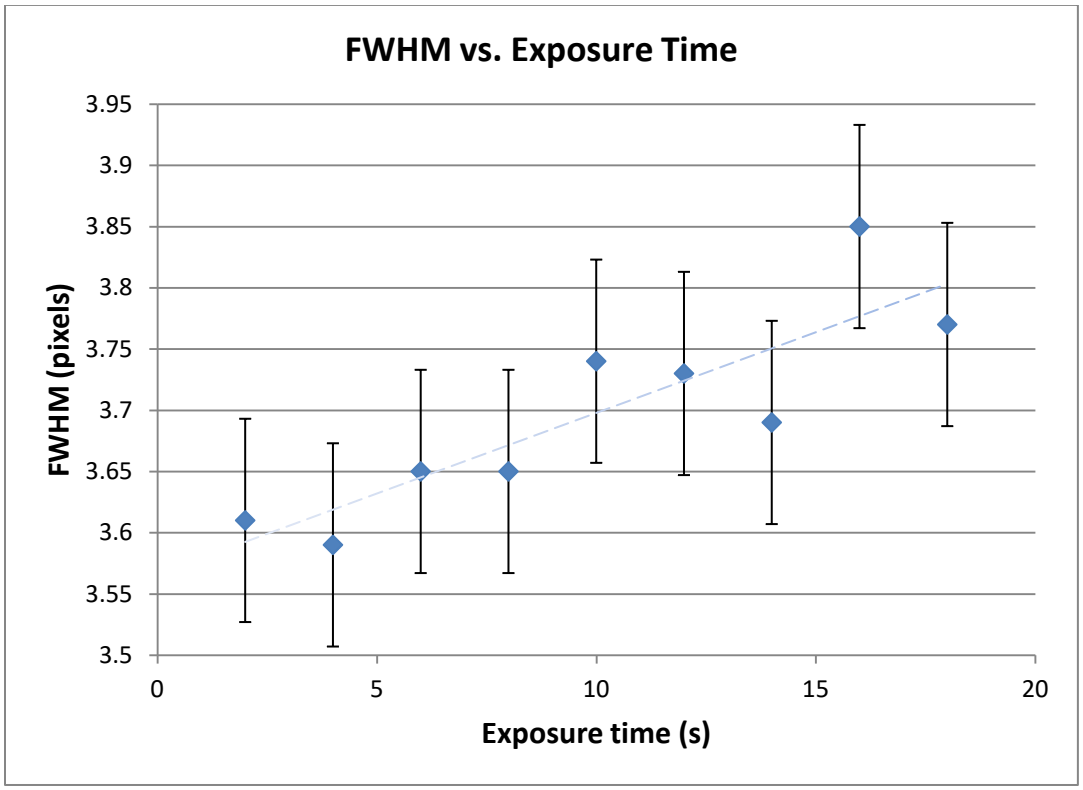

Figure C.2 : FWHM as a function of exposure time.

Because we did not subtract dark frames and hadn't taken any for this exercise, we could not use our star images for photometry. Thanks to Adam McCarron, we were still able to complete our analysis using his exposures of Altair taken with the 24 inch telescope.

For the repeatability measurements, I ran *phot* on a decently bright star (changing the aperture radius to a suitable size) to find its magnitude in each exposure. My results, which include the absolute value of the percent deviations from the mean magnitude (calculated as 100*[measured - mean] / mean), are summarized in Figure C.3 below.

Image	Magnitude	Percent Deviation
1	10.401	0.31340
2	10.400	0.32299
3	10.413	0.19839
4	10.413	0.19839
5	10.429	0.04504
6	10.434	0.00287
7	10.450	0.15622
8	10.458	0.23289
9	10.465	0.29998
10	10.474	0.38624
Average	10.4337	0.21564
StdDev	0.02697	

Figure C.3 : A table summarizing my photometric repeatability measurements.

I'm not sure how to obtain count rates whatsoever. I assume that I would have to use a star with a known flux, then take an image of this source and somehow compare the total DN in the star over the exposure time to the flux.

Exercise D: Color Photometry

Experimental Procedure

We started by slewing to NGC 7686, then began taking test exposures in each of the Johnson B, V and R filters in order to find exposure times that returned maximum DN values in the range 40,000 to 45,000 DN in each filter. We found the optimal B filter exposure time to be 4.75 s, that for the V filter to be 1.5 s and the R 0.975 s. We then planned to take 20 exposures of the cluster in each filter, but cloudy skies forced us to stop after the sixth R filter exposure. See Figure D.4 at the end of this section for samples of these exposures in each filter. When conditions cleared, we slewed to our deep sky target: M27, the Dumbbell Nebula. We planned to take ten 60 s exposures in each filter, but could only obtain eight before the weather prevented us from proceeding once more. We completed the exercise by taking filtered dome flats to later use for flat field corrections on our exposures.

Analysis and Results

I began by mastering the dome flats into single images for each filter. I then corrected the exposures of NGC 7687 for flat field effects and aligned and combined them by following the procedure outlined in Part III of the Pyraf demo. I ran *phot* on 10 target stars (see Fig. D.2) in these three images of the cluster in order to find their magnitudes in each filter. Figure D.1 summarizes my findings. Using this data, I created a number of color-color diagrams and chose to include the (B-V) vs. (B-R) plot (Fig. D.3) in this report.

Star	B magnitude	V magnitude	R magnitude	B-V Index	B-R Index	V-R Index
1	10.101	9.676	9.435	0.425	0.666	0.241
2	11.167	11.168	11.178	-0.001	-0.011	-0.010
3	12.612	12.363	12.079	0.249	0.533	0.284
4	12.975	13.001	12.836	-0.026	0.139	0.165
5	13.009	13.874	13.968	-0.865	-0.959	-0.094
6	12.510	13.373	13.600	-0.863	-1.090	-0.227
7	12.017	12.968	13.349	-0.951	-1.332	-0.381
8	13.144	13.741	13.626	-0.597	-0.482	0.115
9	14.987	14.993	14.781	-0.006	0.206	0.212
10	15.788	15.247	14.908	0.541	0.880	0.339

Figure D.1: Photometry results for the open cluster NGC 7686. Includes B, V and R magnitudes and corresponding indices for a sample of 10 stars in the cluster.

Figure D.2:
Chart labeling the selected stars for my photometric measurements.

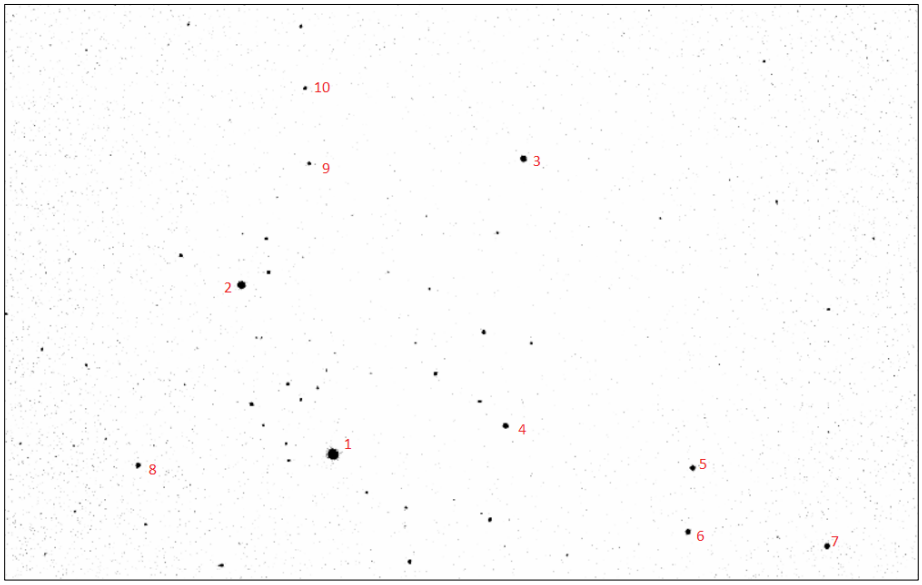

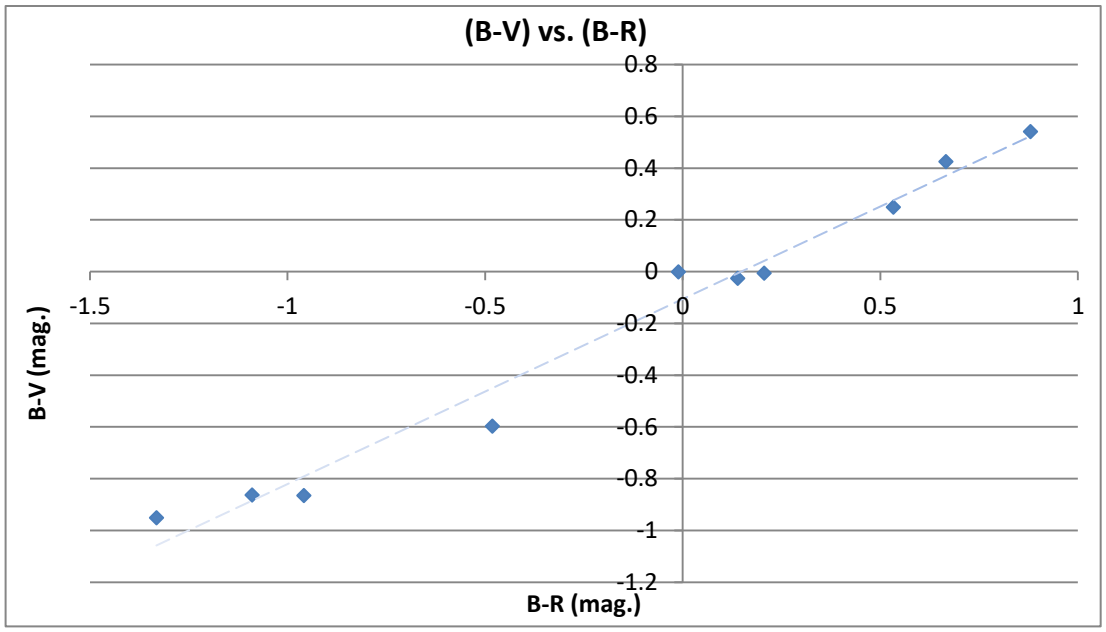

Figure D.3: The (B-V) vs. (B-R) index of the ten sample stars. The trend has a slope of 0.715.

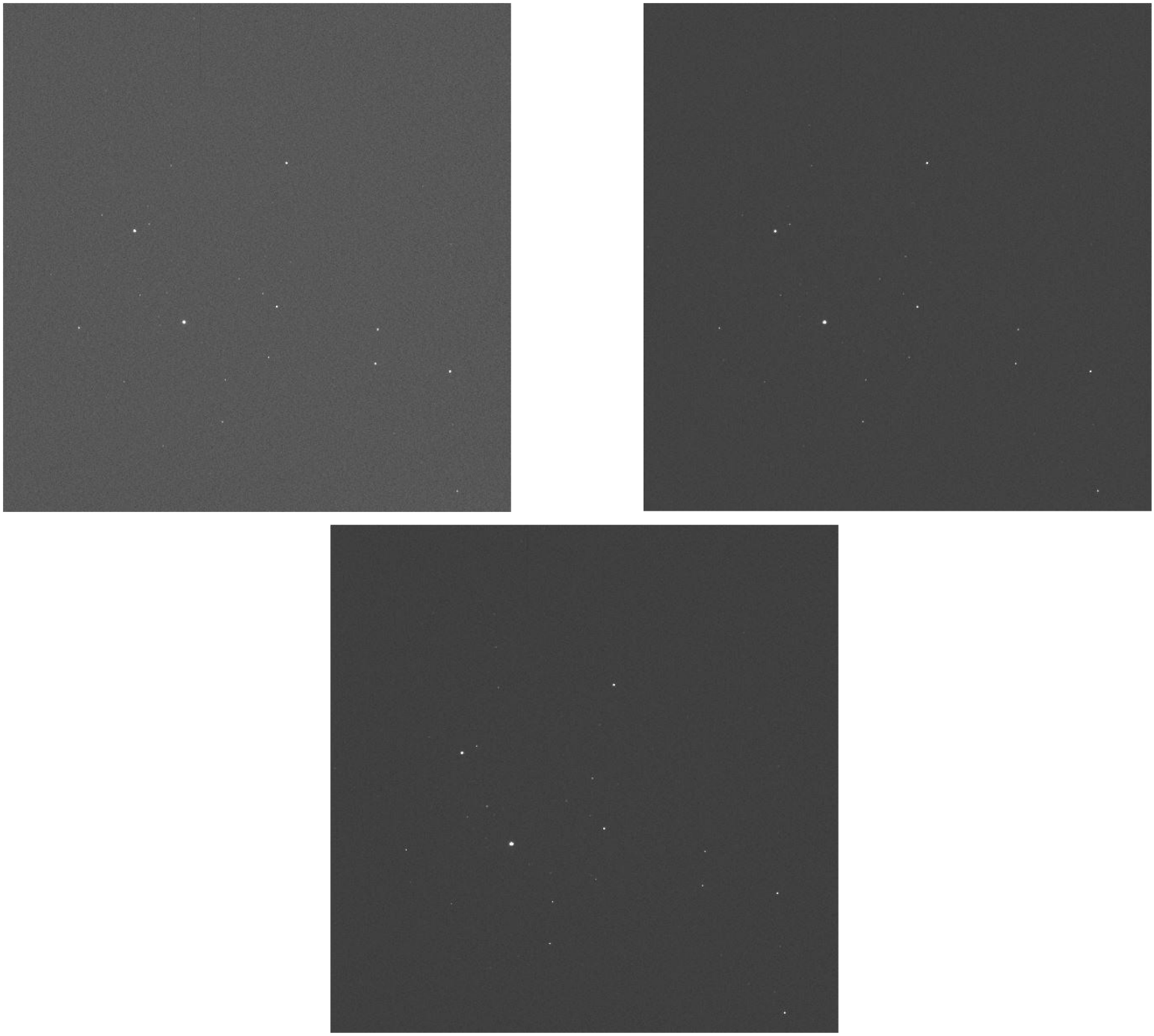

Figure D.4 : Flat-corrected and aligned exposures of NGC7686 in the Johnson B (left), V (right) and R (bottom) filters.

Using Nebulosity, I flat-corrected, aligned and combined our exposures of Messier 27 in each filter. Figure D.5 below shows the three master images in the B, V and R filters.

Figure D.5 : Exposures of M27 flat corrected and aligned using Nebulosity for 4.75 s in the B filter (left), 1.5 s in the V filter (center) and 0.975 s in the R filter (right).

I then aligned and combined *these* images with each other to form the color image shown in Figure D.6. This image shows clearly the central star of the nebula, a white dwarf with a radius of $0.56 \pm 0.01\ M_{\odot}$(Benedict et. al 2003). The green (higher energy) hue of the nebula near the central star is indicative of ionized gas, and I would guess that the red (lower energy) ends of the "dumbbell" are indeed the dissipating remainder of the former star's outer layers. Other than the nebula, the image shows one obvious binary system at the top right, and a very bright red star (perhaps a red giant) in the bottom left quadrant.

Figure D.6 : The composite RGB image of the Dumbbell Nebula made in Nebulosity. The tear seen at the bottom of the image is likely due to a flat-correcting error.

Exercise E: Measuring the Plate Scale of the CCD Camera

Experimental Procedure

In preparation for this exercise, we set up an AstroPlanner file (Fig. E.1) listing information regarding 15 double stars that we could potentially use for our observations. Due to technical issues and cloud cover, we only had time to slew to five of our candidates and could only take exposures of four. We experimented with different filters and exposure times for each candidate in order to achieve the best looking images, thereby getting better results. We took a 12 s exposure of 17 Draconis in the Oxygen III filter, a 1 s exposure of β Cygni in the Hα filter, a 20 s exposure of 8 Lacertae in the Oxygen III filter and a 5 s exposure of 56 Andromedae in the V filter.

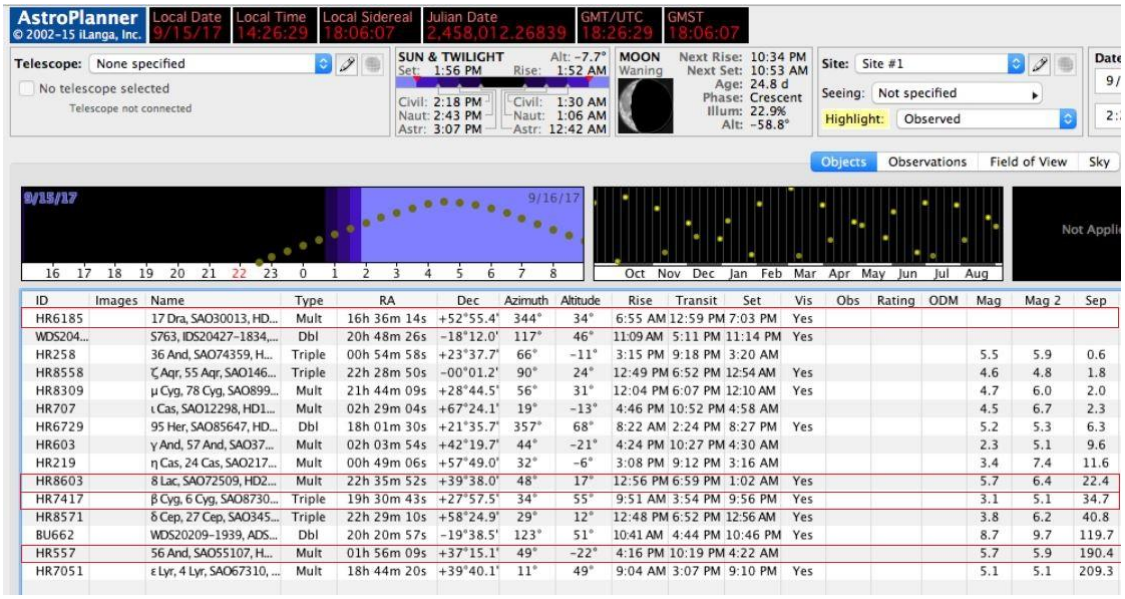

Figure E.1 : The AstroPlanner file used for our observations.

Analysis and Results

We completed the task of measuring the stars' separations on the CCD by the following means:

1. Manually find the approximate coordinates of the endpoints of the star's diameter along its horizontal axis, the difference in these coordinates is the approximate diameter in pixels.
2. Adjust centerpars settings such that the value for cbox is larger than the star's diameter in pixels and maxshift is half of the value of cbox.
3. Centroid the stars using *phot* → [*SPACE*]; write down their center coordinates.
4. Find the differences in the coordinates of the two stars; use the Pythagorean Theorem to find their net separation in pixels.

Dividing the pairs' angular separations by their CCD separations resulted in estimates of the plate scale ("/pixel) (Fig. E.2). There were no outliers in the data, and intuition tells me that the actual plate scale of the telescope is 0.7 "/pixel even though this value is not within our standard deviation. Errors in my

Pair Name	Angular Separation (")	CCD Separation (pixels)	Plate Scale ("/pixel)	Mean Plate Scale ("/pixel)
8 Lacertae	22.4	31.98	0.70044	0.70074 ± 0.00022
β Cygni	34.7	49.52	0.70073	
17 Draconis	90.3 (Inglis 2012)	128.84	0.70087	
56 Andromedae	203.8	290.76	0.70092	

Figure E.2 : The results of my analysis for this exercise.

As expected, plotting the CCD separations as a function of angular separations (Fig. E.3) on the sky consistently shows the linear relationship between the two quantities for each pair. The standard deviation from the mean plate scale (0.00022 "/pixel) is used as the error on the plot.

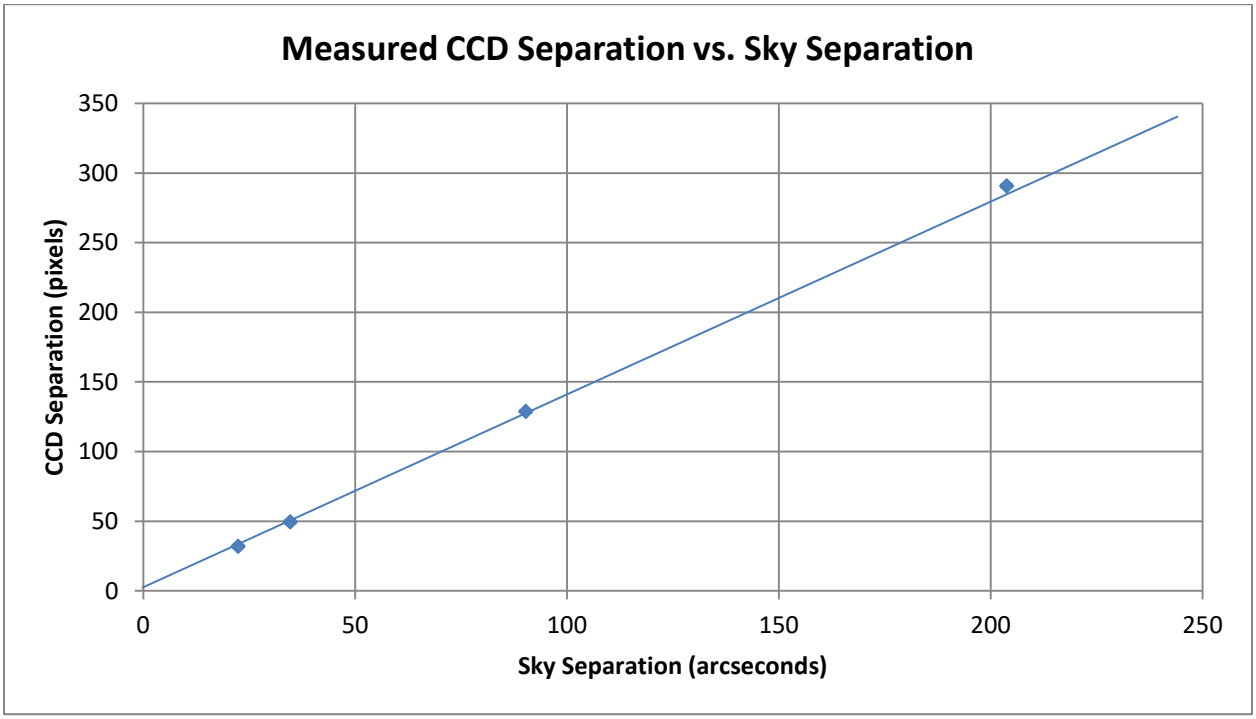

Figure E.3 : The separation on the CCD that I measured vs. the actual separation on the sky.

I found the typical seeing during our observations to be 3.66" (Category II seeing). To determine this, I used *imexam* → [*Period*] to find the FWHM of both stars in each system, then averaged these values and multiplied by the mean plate scale.

Images produced by the CCD have dimensions of 2048 x 2048 pixels. Multiplying by the plate scale, I found that the telescope has a field of view of around 1435 x 1435 " or 23.92 x 23.92 arcminutes.

References

Benedict, G. Fritz; McArthur, B. E.; Fredrick, L. W.; Harrison, T. E.; et al. (2003). "Astrometry with The Hubble Space Telescope: A Parallax of the Central Star of the Planetary Nebula NGC 6853". *Astronomical Journal*; p. 126.
(Benedict et. al 2003)

Inglis, MD. 2012. "A Field Guide to Deep-Sky Objects". Second Edition. New York (NY): *Springer Science and Business Media*; p. 96.
(Inglis 2012)